

1 A digital twin for DNA data storage 2 based on comprehensive quantification 3 of errors and biases 4

5 Andreas L. Gimpel¹, Wendelin J. Stark¹, Reinhard Heckel², Robert N. Grass^{1*}

6 ¹ Department of Chemistry and Applied Biosciences, ETH Zürich, Vladimir-Prelog-Weg 1-5, 8093,
7 Zürich, Switzerland

8 ² Department of Electrical and Computer Engineering, Technical University of Munich, Arcistrasse 21,
9 80333, Munich, Germany

10 * robert.grass@chem.ethz.ch

12 **Keywords**

14 error correction coding, channel model, DNA data storage, DNA errors, polymerase chain reaction,
15 sequencing-by-synthesis, amplification bias, synthesis bias, sequencing coverage,

16 **Abstract**

18 Archiving data in synthetic DNA offers unprecedented storage density and longevity. Handling and
19 storage introduce errors and biases into DNA-based storage systems, necessitating the use of Error
20 Correction Coding (ECC) which comes at the cost of added redundancy. However, insufficient data on
21 these errors and biases, as well as a lack of modelling tools, limit data-driven ECC development and
22 experimental design. In this study, we present a comprehensive characterisation of the error sources
23 and biases present in the most common DNA data storage workflows, including commercial DNA
24 synthesis, PCR, decay by accelerated aging, and sequencing-by-synthesis. Using the data from 40
25 sequencing experiments, we build a digital twin of the DNA data storage process, capable of simulating
26 state-of-the-art workflows and reproducing their experimental results. We showcase the digital twin's
27 ability to replace experiments and rationalize the design of redundancy in two case studies,
28 highlighting opportunities for tangible cost savings and data-driven ECC development.

29

Introduction

30 As the amount of digital data to be stored continues to grow by Zettabytes every year, DNA is
31 considered as a potential alternative to conventional storage media due to its exceptional stability and
32 storage density.^{1–5} The use of DNA as storage medium presents unique practical challenges, such as
33 affordability and scalability, as well as design challenges, such as the choice of redundancy and
34 algorithm for error correction coding (ECC).^{3,6,7} The latter challenge is aggravated by the errors
35 incurred by data stored in DNA, ranging from single-site errors (i.e., substitutions, deletions, and
36 insertions) to sequence dropout (i.e., the loss of data-encoding sequences).⁶ While errors stem directly
37 from the chemical or biological processes involved in the DNA data storage workflow (e.g., synthesis,
38 amplification, aging, and sequencing), sequence dropout is the product of a biased distribution for the
39 oligonucleotide count per sequence (i.e., the coverage distribution). Due to these errors and biases,
40 data stored in DNA is encoded with redundancy using ECC.^{6,8,9} These coding schemes add redundancy
41 to recover the encoded data from the DNA sequences while correcting a limited number of errors and
42 tolerating some missing sequences. However, choosing the optimal level of redundancy requires *a*
43 *priori* knowledge of the expected error and dropout rates, for which insufficient experimental data are
44 available. Instead, experience and overcompensation currently guide the choice of parameters.

45 Beyond just choosing an adequate redundancy level, choosing a suitable ECC from the many
46 implementations reported to date^{8,10–13} requires standardized error scenarios facilitating meaningful
47 and fair comparisons. Computational comparisons have relied on fictitious error scenarios^{12,13} –
48 considering error types in isolation – while experimental comparisons are costly and potentially
49 misleading due to the plethora of potentially critical experimental parameters. *In-silico* tools for the
50 simulation of errors in DNA exist,^{14–16} but they often do not support the parallel simulation of large
51 oligonucleotide pools, neglect sequence dropout due to evolving bias in the coverage distribution, or
52 directly reproduce experimental error patterns without considering experimental parameters. To
53 replace experiments or compare ECCs however, an *in-silico* tool for DNA data storage must accurately
54 reflect the errors and sequence dropout of state-of-the-art workflows based only on experimental

55 parameters. This requires a systematic understanding of the individual sources of errors and biases
56 encountered in such workflows.

57 Many of the biological and synthetic methods used in common DNA data storage workflows are well
58 characterized (e.g. oligonucleotide synthesis^{17,18}, PCR^{19,20}, sequencing-by-synthesis (SBS)^{21,22}). In
59 contrast, studies on DNA data storage often only quantify overall error rates – if at all – and do not
60 consider coverage biases. The works by Heckel et al.⁶ and Chen et al.²³ began quantifying these error
61 sources in isolation, identifying significant biases related to the synthesis and amplification of
62 oligonucleotide pools. Still, no study has systematically investigated the evolution of error rates and
63 coverage biases throughout the entire DNA data storage workflow.

64 In this work, we comprehensively characterise the error sources and biases present in the most widely-
65 used DNA data storage workflows to date.^{1,9} This includes commercial DNA synthesis from the two
66 major providers of large-scale oligonucleotide pools used in the literature¹ (i.e., Twist Biosciences and
67 Genscript/CustomArray), amplification via PCR, long-term storage and decay by accelerated aging, and
68 sequencing by Illumina’s SBS technology. For our investigation, we systematically sequenced
69 oligonucleotide pools throughout the workflows to analyse their error profiles and coverage
70 distributions, for a total of 40 sequencing datasets. By characterising the base preferences, positional
71 dependencies, and distributional inhomogeneities of all errors, we provide a complete description of
72 all error sources in the various steps of the workflows. In addition, the analysis of coverage
73 distributions revealed any potential coverage bias from synthesis, amplification, and aging, which we
74 show to be critical for understanding sequence dropout. Finally, we condense the data on error rates
75 and biases into a digital twin of the DNA data storage process: a tool to explore experimental workflows
76 and provide standardized simulations for experimental scenarios. We demonstrate the digital twin’s
77 ability to reproduce state-of-the-art workflows and showcase its application to the data-driven design
78 of redundancy, which offers opportunities to replace costly experiments and facilitate meaningful
79 comparisons between ECCs.

80 **Results**

81 In this work, we characterize errors and biases from sequencing data using four oligonucleotide pools,
82 each with 12000-12472 sequences of 143-157 nucleotides (nt). Two pools were synthesized via an
83 electrode array-based method (Genscript/CustomArray) and two by a material deposition-based
84 technology (Twist Biosciences). All pools consisted of random sequences, with one pool each enforcing
85 a constraint on GC-content of 50% (“GC-constrained”), while the other remained unconstrained (see
86 Methods and Supplementary Table 1). All pools were used in two workflows, consisting of either
87 extensive reamplification with up to 90 PCR cycles or accelerated aging up to an equivalent storage
88 duration of 1000 years at 10°C. Throughout the process, samples of the pools were sequenced to track
89 the evolution of errors and biases for a total of 40 experimental endpoints across the two workflows.
90 For our analysis, errors and biases were characterized by aligning sequencing reads to their respective
91 references, identifying mutations, and evaluating the resulting error patterns. For more details on the
92 analysis procedure and the datasets used, we refer to the Methods and Supplementary Note 1.

93 In the following, we first quantify the overall error rates in our experiments, followed by the
94 characterization of each individual error source in the data storage workflow. We then build and verify
95 a computational model of the workflow, which is used in a case study to illustrate its value for the
96 data-driven choice of redundancy in ECCs.

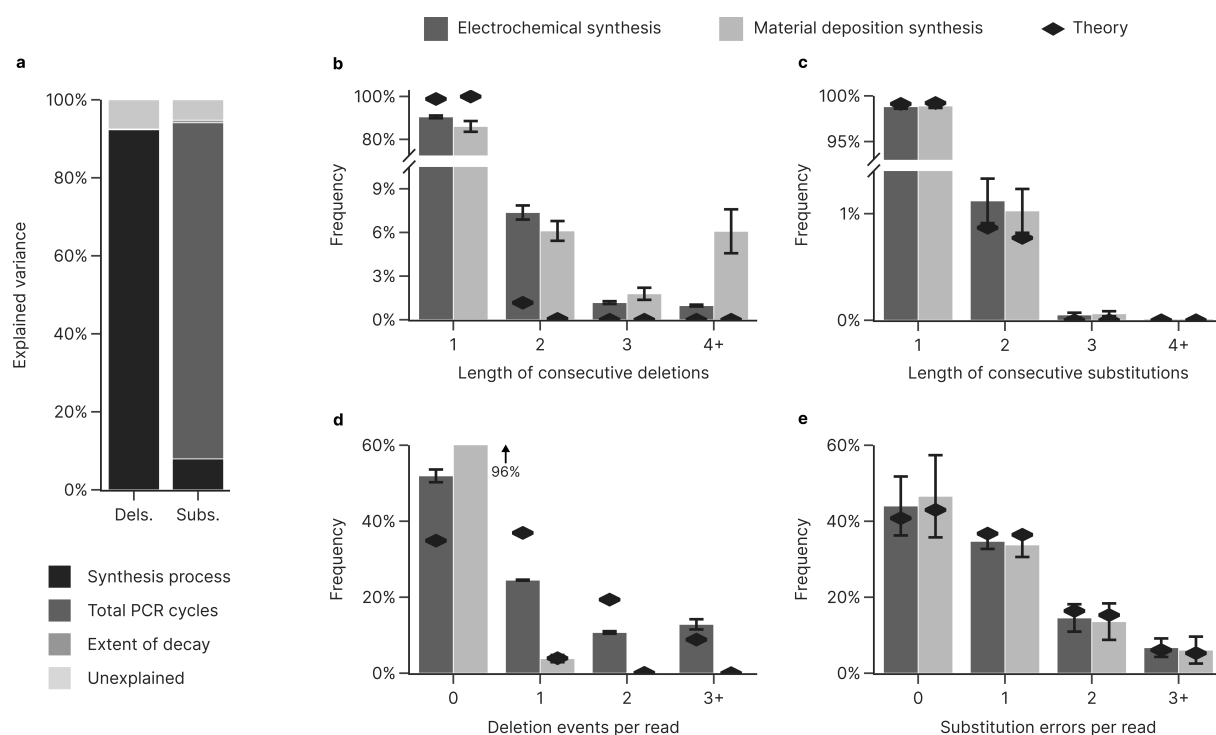
97 **Identifying error sources and assessing error independence**

98 To validate our experimental approach, we first compared our overall error rates to those published
99 in previous studies. Throughout all our 40 datasets, we observed overall error rates of 6.7 ± 6.9
100 deletions, 7.9 ± 2.0 substitutions, and $<0.3 \pm 0.2$ insertions per thousand nucleotides (i.e., 10^{-3} nt⁻¹) on
101 average, in-line with error rates published in other studies.^{6,24,25} Variation in the observed deletion and
102 substitution rates between different experimental conditions and different oligonucleotide pools was
103 large, with maximum rates of $17.1 \cdot 10^{-3}$ nt⁻¹ deletions and $12.5 \cdot 10^{-3}$ nt⁻¹ substitutions, respectively.
104 Analysing the variance across the measured error rates in this diverse dataset (three-way ANOVA with
105 HC3 correction, see Fig. 1a) – considering synthesis provider, number of PCR cycles, and storage

106 duration as factors in a main effects analysis – showed that synthesis and PCR were the major error
107 sources in our experiments. The synthesis process explains most of the difference observed in deletion
108 rates ($F(1, 76) = 933.7, p = 10^{-44}$), accounting for 92% of its variance. This highlights synthesis as a
109 dominating source of deletions, as noted by others,^{17,18} and identifies a large difference in fidelity
110 between synthesis processes. In contrast, substitution rates varied most between samples with
111 different sample preparations. PCR was found to be the main factor affecting substitutions ($F(1, 76) =$
112 $1251, p = 10^{-49}$), accounting for 86% of the variance (see Fig. 1a). The full ANOVA results are presented
113 in Supplementary Table 8.

114 Next, we assessed error independence in our datasets, i.e. the assumption that mutations occur
115 independently from one to another, which is often inherently assumed when modelling errors in
116 DNA.^{12,13,15} To do so, we compared the frequency distributions of consecutive errors and errors per
117 read to those expected assuming that errors are introduced independently. Under error
118 independence, we expect to observe consecutive errors according to a geometric distribution with
119 success probability equal to the average error rate. We found that, while the frequency of consecutive
120 substitutions closely matches its theoretical distribution (see Fig. 1c), the occurrence of multiple
121 consecutive deletions was considerably more frequent (see Fig. 1b). Runs of consecutive deletions –
122 with a mean length of 2.6 bases and referred to as a deletion event – were overrepresented and
123 accounted for 10-14% of all deletions, depending on the synthesis process. Going further, the
124 frequency distribution of errors per read is expected to be binomially distributed under the assumption
125 of error independence, with the length of the sequence and the average error rate as parameters.
126 Substitutions showed good agreement to this theoretical distribution (see Fig. 1e), whereas deletion
127 events behaved differently depending on synthesis technology (see Fig. 1d). For electrochemical
128 synthesis, deletion events were heavily clustered in a small subset of reads. While this led to a greater
129 proportion of deletion-free reads (52% vs. 35% expected) and a small number of reads with only one
130 or two deletions (35% vs. 56% expected), about 13% (vs. 9% expected) of oligonucleotides in these
131 pools featured at least three deletions. No clustering across reads was evident for the material

132 deposition-based synthesis, as deletions were generally rare. Taken together, this analysis established
133 that the assumption of error independence is generally valid for substitutions, but is violated for
134 deletions, which tend to cluster both within and across reads in the electrochemical synthesis.



135
136 **Fig. 1: Overview of error variance and general error distributions.** (a) The contributions of synthesis process, PCR cycles, and
137 extent of decay to the overall variance in mean deletion (left) and substitution (right) rates between samples were assessed
138 by four-way analysis of variance (ANOVA, see Methods and Supplementary Table 8). (b-e) Distributional analysis of error
139 independence for deletions (b+d) and substitutions (c+e) based on the observed frequency of error runs (b+c) and errors per
140 read (d+e), for the GC-unrestricted pools synthesized by electrochemical (dark grey) and material deposition (light grey)
141 processes. Theoretical distributions expected under the assumption of error independence are also shown (black diamonds,
142 geometric/binomial). The histogram for deletions per read treats any run of deletions as a single event to accommodate the
143 non-ideality of deletion runs. Error bars show the standard deviation of the sample.

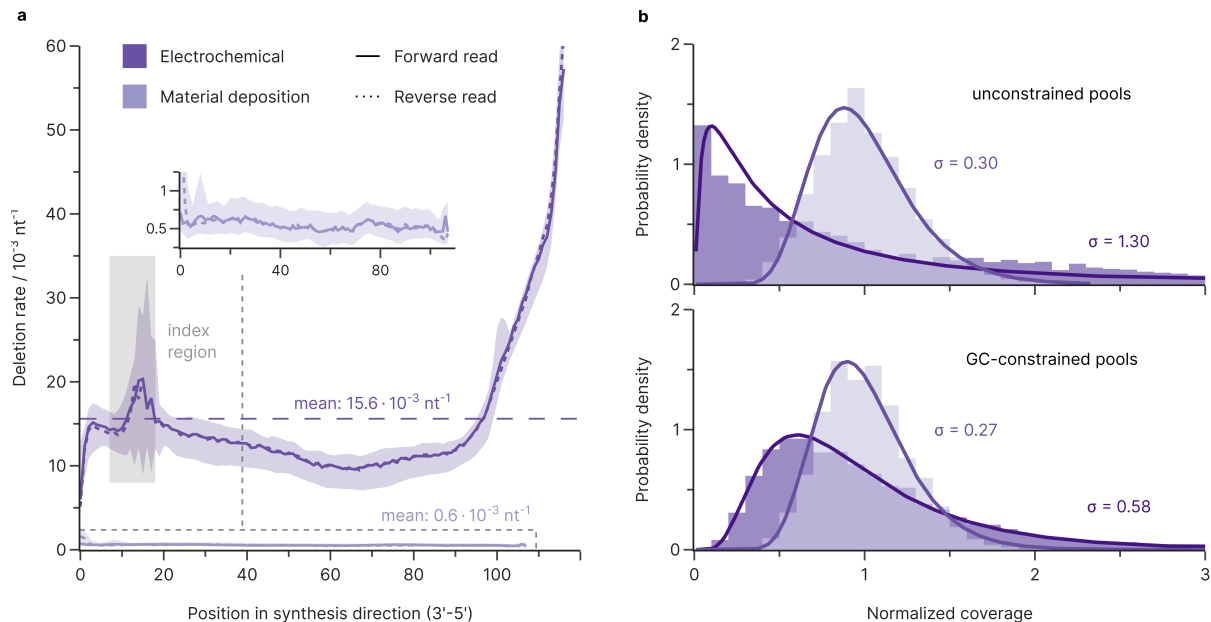
144 **Not all DNA is created equal: synthesis errors and coverage biases**

145 As noted above, the large difference in mean deletion rate between electrochemical ($13.5 \pm 2.0 \cdot 10^{-3} \text{ nt}^{-1}$)
146 and material deposition-based ($0.58 \pm 0.15 \cdot 10^{-3} \text{ nt}^{-1}$) synthesis identified synthesis as the main error
147 source for deletions. This is corroborated by the positional dependence of deletions in the sequencing
148 reads, which showed a distinct increase in the synthesis direction for the electrochemical synthesis
149 (i.e., 3'-5' for the forward read, 5'-3' for the reverse read, Fig. 2a). The strongly increasing deletion rate

150 observed towards the 5'-end of the electrochemically synthesized oligonucleotides, >5% per
151 nucleotide, likely stems from mass-transfer limitations. As the synthesized oligonucleotide becomes
152 longer, the distance to the acid-generating electrode grows and steric hindrance increases the
153 electrochemical cell resistance, impeding acid-induced deprotection and preventing both subsequent
154 addition of the next nucleotide and blocking of the erroneous oligonucleotide by capping.^{26,27} This also
155 explains the observed deviation from statistical independence for deletions noted previously:
156 oligonucleotides which have already suffered from mass transfer-induced deletions are more likely to
157 do so again in subsequent deprotection steps, leading to a cluster of deletions. Material deposition-
158 based synthesis on the other hand exhibited neither a high deletion rate nor any considerable
159 positional dependence. With a fidelity exceeding one deletion error in 2000 nucleotides, these
160 amplified oligonucleotides were essentially error-free for the purposes of DNA data storage. Despite
161 this large difference in deletion rates, both synthesis processes find broad application in DNA data
162 storage,¹ likely due to considerations of scalability and cost. For both synthesis processes, deletions
163 also did not show any relevant bias towards any nucleotide, and only a negligible number of
164 substitutions were introduced (see Supplementary Note 3).

165 Focussing on the coverage distributions of the oligonucleotide pools after synthesis, we compared
166 sequencing data obtained after minimal sample preparation (15 PCR cycles and size selection by
167 agarose gel electrophoresis). Similar to other studies,^{8,23} the normalized coverage distributions of all
168 oligonucleotide pools in our study were positively skewed – featuring a long tail of few sequences at
169 high coverages – and were well approximated by lognormal distributions (see Fig. 2b). Quantifying this
170 coverage bias with the standard deviation of the corresponding lognormal distribution (σ) highlighted
171 the severe effects of the GC-constraint on the electrochemically synthesized pools. While synthesis by
172 material deposition yielded near-gaussian coverage both with unconstrained and GC-constrained
173 sequences ($\sigma = 0.27$ vs. $\sigma = 0.30$), electrochemical synthesis yielded slightly biased coverage with
174 GC-constrained sequences ($\sigma = 0.58$), and severe bias without constraints ($\sigma = 1.30$, see Fig. 2b).
175 Combined with the significant difference in mean deletion rates between these synthesis methods,

176 the choice of synthesis provider critically affects the baseline error level and coverage bias for DNA
177 data storage.



178
179 **Fig. 2: Errors and biases from synthesis.** (a) Median deletion rate over all experiments as a function of position in synthesis
180 direction, grouped by synthesis process and read direction. The deletion rate is strongly position-dependent for
181 electrochemical synthesis (dark purple) but negligible for DNA synthesized via material deposition (light purple, magnified in
182 inset). Both forward (solid lines) and reverse reads (dotted lines) are shown, each in synthesis direction, for all samples
183 irrespective of their sample preparation. Shaded areas enclose all datapoints from the set, e.g., from minimum to maximum.
184 Co-synthesized priming regions flanking the data-encoding bases are not considered, as PCR is expected to select for error-
185 free priming regions.²⁴ Mean deletion rates over all positions (dashed line) and the indexing region (shaded in grey), where
186 the sequences have very low diversity, are also shown. (b) Coverage distributions normalized to the mean coverage for
187 oligonucleotide pools with (bottom) and without (top) constraints on GC content from electrochemical (dark purple) and
188 material deposition-based synthesis (light purple) after 15 PCR cycles. All pools fit a lognormal distribution (solid line), but
189 the material deposition-based pools show more even oligonucleotide coverage for both pool types. Standard deviations of
190 the fitted lognormal distributions are shown in the plot.

191 **Quantifying substitutions and bias introduced via PCR**

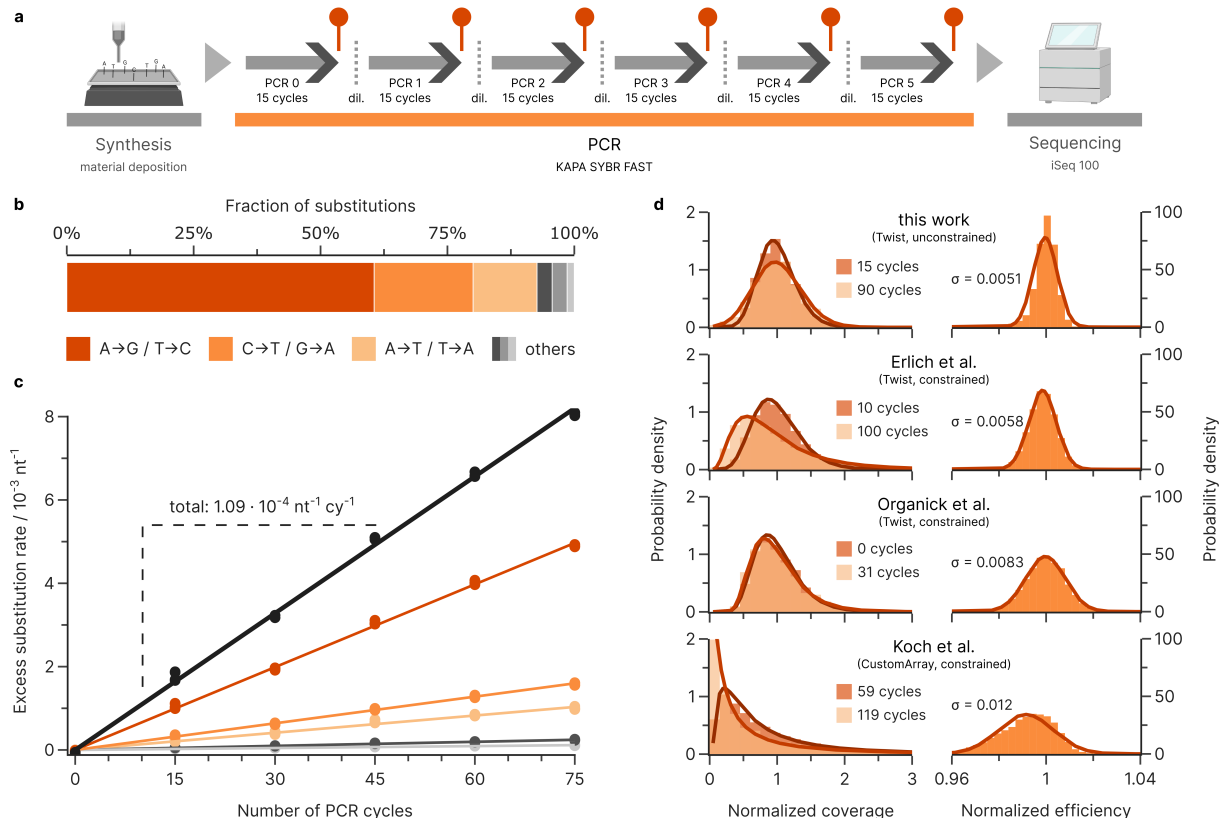
192 Generally, PCR introduces both substitution errors and biases into oligonucleotide pools, mainly due
193 to the limited fidelity of the polymerase.^{6,23} Previous studies have characterized PCR errors in the
194 context of genomic sample amplification (e.g. for mutation detection via high-throughput
195 sequencing),^{19,20} but PCR errors are also relevant for DNA data storage, where they reduce the fraction

196 of error-free oligonucleotides. To assess this, we characterized the errors introduced during PCR by
197 amplifying samples of the oligonucleotide pools with varying numbers of PCR cycles and quantifying
198 the evolution in error rates (see Fig. 3a). All PCR experiments were stopped well before reaching the
199 plateau phase to ensure an excess of primers and nucleotides for exponential amplification.
200 Sequencing data showed that PCR introduced only substitutions, at a mean rate of $1.09 \cdot 10^{-4}$ nt⁻¹ cycle⁻¹
201 for our Taq-based polymerase (KAPA SYBR FAST), see Fig. 3b and Fig. 3c. The polymerase exhibited
202 a strong bias towards A→G/T→C transitions (61% of substitutions), with further preference for
203 A→T/T→A transversions (13%). This is in-line with the studies quantifying polymerase fidelity based
204 on single amplicons, which found substitution rates within $1 \cdot 10^{-5}$ to $2 \cdot 10^{-4}$ nt⁻¹ cycle⁻¹ for Taq-
205 polymerase, and similar substitution patterns.^{19,20,28} Consequently, the established polymerase fidelity
206 metric (i.e. polymerase fidelity relative to Taq-polymerase) can be used to extrapolate the substitution
207 rates expected from other commonly-used polymerases in the context of DNA data storage.^{19,20} The
208 C→T/G→A transition was also relevant in our experiments (19% of substitutions), but is thought to
209 occur due to temperature-induced cytosine deamination during thermocycling rather than polymerase
210 errors.²⁰

211 Stochastic effects of PCR and non-uniform amplification lead to biases in coverage distributions.^{6,23,29–}
212 ³¹ To quantify this amplification bias in a DNA data storage context, we characterized the distribution
213 of normalized amplification efficiencies, i.e. the ratio $\frac{1+\epsilon_i}{1+\bar{\epsilon}}$ between an individual sequence's efficiency,
214 $\epsilon_i \in [0,1]$, and the pool's mean efficiency, $\bar{\epsilon}$, for our datasets. Assuming negligible stochastic effects
215 (i.e., at high initial coverage), the relative amplification efficiency is related to the experimentally-
216 observed fractional change in normalized sequence coverage, x_i , from sequencing before and after
217 amplification with c cycles:³¹

$$218 \frac{1+\epsilon_i}{1+\bar{\epsilon}} = \left(\frac{x_i(c)}{x_i(0)} \right)^{\frac{1}{c}}.$$

219 We found that the relative amplification efficiencies are normally distributed in our material
220 deposition-based oligonucleotide pools, with a standard deviation of 0.0051 (unconstrained pool) and
221 0.0048 (GC-constrained pool), see Fig. 3d and Supplementary Figure 13. To validate our estimate of
222 the overall PCR bias, we replicated this analysis for the sequencing data reported by Chen et al.²³
223 (change of 31 PCR cycles), Erlich et al.⁸ (90 cycles), and Koch et al.²⁵ (60 cycles). We found amplification
224 biases which were larger, but comparable to ours (see Fig. 3d), with standard deviations ranging from
225 0.0058 to 0.012. Given these datasets, the broadness of the efficiency distribution does not appear to
226 directly depend on GC constraints and is thus likely caused by experimental conditions. To this end,
227 factors such as the choice of primer, the temperature and duration of the steps, or the polymerase
228 itself are known to affect amplification efficiency and thus amplification bias, amongst others.³²⁻³⁵
229 Specifically the use of high-fidelity, proofreading polymerases (such as by Erlich et al.⁸ and Organick et
230 al.²³), which stall DNA synthesis upon reading uracil, might incur a stronger amplification bias due to
231 cytosine deamination to uracil during storage.³⁶ Moreover, the repeated dilutions needed after each
232 amplification, albeit performed at high physical coverage, will introduce stochastic effects. The data by
233 Koch et al.²⁵ is an extreme example of this: after amplification, the DNA was incorporated into silica
234 nanoparticles embedded in polymer. For these reasons, the empirical distributions of the relative
235 amplification efficiencies should be interpreted as an upper bound of the true amplification bias.
236 Due to the exponential nature of PCR, the normally distributed amplification efficiency leads to a
237 progressively more positively skewed coverage distribution with a long tail (see Fig. 3d). This initially
238 small effect thus gains relevance as many amplifications are performed, in-line with observations in
239 literature.^{30,37} Considering that data storage workflows routinely use >60 PCR cycles and pools might
240 already be highly skewed from synthesis (see Fig. 2b), PCR considerably biases the oligonucleotide
241 pool. Thus, the efficiency bias presents a constraint on the number of re-amplifications that a DNA
242 data storage system may go through before the uneven coverage distribution either prevents
243 successful decoding or necessitates higher physical coverage and sequencing depth.^{6,23}



244

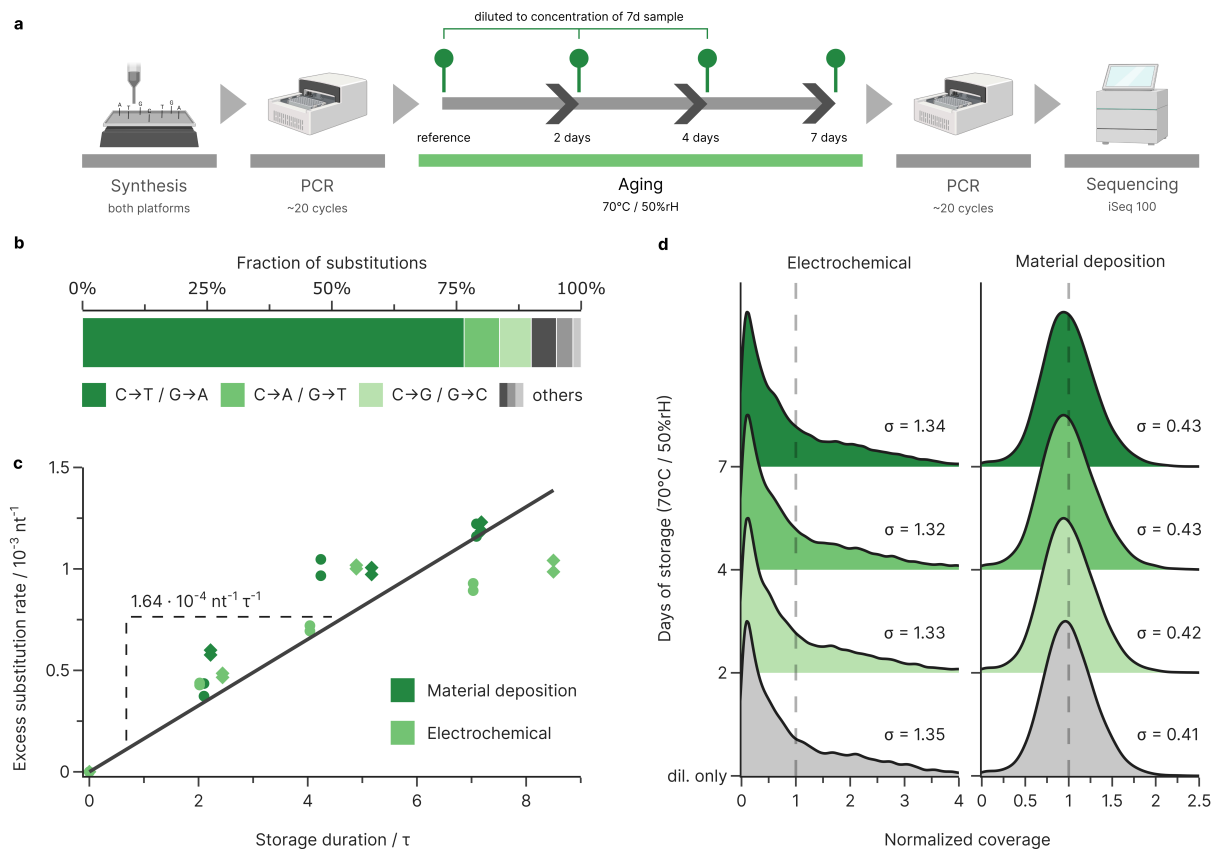
245 **Fig. 3: Errors and biases from PCR.** (a) Experimental workflow for estimating the error rates and biases during PCR. (b+c)
246 Substitutions introduced as a function of the number of additional PCR cycles for the oligonucleotide pools from material
247 deposition-based synthesis, using the substitution rate at 15 cycles as the baseline. The regression slope (solid lines) yields
248 an overall error rate of $1.09 \cdot 10^{-4} \text{ nt}^{-1}$ per cycle and shows A→G/T→C transitions account for 61% of substitutions, followed
249 by C→T/G→A transitions (20%) and A→T/T→A transversions (13%). (d) The normalized coverage distributions (left) of
250 sequencing pools shown before (dark orange) and after repeated amplification (light orange). Without any PCR bias, the post-
251 PCR coverage distributions are expected to be identical to the pre-PCR distributions. Relating the change in coverage pre- and
252 post-PCR to the number of PCR cycles on the sequence level yields an estimate of the efficiency relative to the pool (right).
253 The broadness of the resulting efficiency distribution, characterized by the standard deviation of the fitted normal
254 distributions given in the plots (solid lines), can be interpreted as an upper bound on the overall PCR bias. Comparison shown
255 of efficiency distributions between our experiments, the deep amplification performed by Erlich et al.⁸, the bias experiment
256 by Organick et al.²³, and the bunny experiments by Koch et al.²⁵. Individual sequences with less than 10 reads in the
257 sequencing data were removed from this analysis, due to the large uncertainty associated with sampling at low coverage.

258

259 **Quantifying errors during storage**

260 The detrimental impact of long-term storage on DNA data storage systems is well established, and
261 usually quantified by the loss of amplifiable DNA over time.^{7,38,39} Here, in addition to quantifying this
262 loss of DNA, we also tracked the evolution of errors and biases during rapid aging by sequencing the
263 oligonucleotide pools at various storage durations, up to the equivalent of more than 1000 years at
264 10°C (7 days at 70°C, see Fig. 4a). We observed a linear increase in C→T and G→A transitions as the
265 major type of substitution errors, with around $1.64 \cdot 10^{-4}$ nt⁻¹ per half time of decay overall (see Fig. 4b
266 and c). In addition, a small number of deletions were introduced. These were negligible compared to
267 the deletions present due to the synthesis (see Supplementary Figure 14). Overall, the measured error
268 rates show that storage-induced decay is not a significant error source in the context of DNA data
269 storage. Comparing to other error sources, storage for eight half-lives – equivalent to the loss of 99.6%
270 of DNA – introduces less errors than just 15 cycles of standard, Taq-based PCR. Therefore, the main
271 effect of storage-induced decay is limited to the loss of sequences, and we focussed on characterising
272 any possible bias in this loss.

273 To assess the overall bias in decay, we compared the coverage distributions between aged samples
274 and an equally diluted and amplified, but unaged, reference. We observed no difference in the
275 coverage of aged samples compared to unaged, but diluted samples (see Fig. 4d), meaning decay did
276 not introduce considerable additional bias over random sampling. Thus, the impact of decay on
277 coverage distribution is well approximated by random sampling and any potential bias is likely
278 secondary to the stochastic effects from sampling at low physical coverage. As aging neither
279 introduced errors at relevant rates, nor significantly affected the coverage distribution in our
280 experiments, recovered oligonucleotides (i.e., those without strand breaks induced by β-elimination)
281 remained virtually unaffected by decay. This implies that long-term storage does not negatively impact
282 the error resilience or fidelity, as long as sequence dropout is limited by sufficient coverage or
283 enzymatic repair.³⁸



284

285 **Fig. 4: Errors and biases during storage.** (a) Experimental workflow for estimating the error rates and biases during aging.

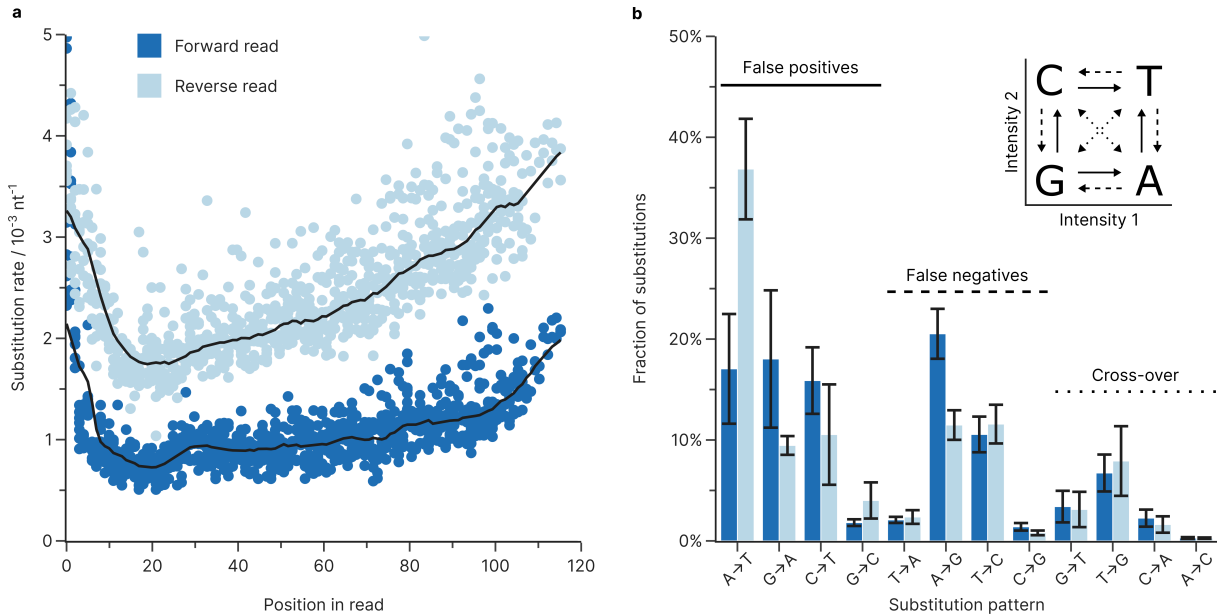
286 (b+c) Substitutions introduced as a function of the total storage duration in half-lives, using the error rates of the unaged
 287 reference as baseline. Substitutions increase at a rate of $1.64 \cdot 10^{-4} \text{ nt}^{-1}$ per half-live based on the regression slope (solid line).
 288 Substitutions are mainly C → T/G → A transitions (dark green, 77%) with minor C → A/G → T and C → G/G → C transversions (7%
 289 and 6% respectively). (d) Kernel density estimate plot of the oligonucleotide coverage for the GC-unconstrained samples
 290 which were only diluted (grey), and samples which underwent decay for 2-7 days (green), for both electrochemical (left) and
 291 material deposition-based synthesis (right). All samples were diluted to the same concentration prior to amplification. The
 292 grey distribution shows the effect of subsampling via dilution, whereas the other distributions show the combined effects of
 293 dilution and decay. The standard deviations of the lognormalized distributions are given in the plot.

294 **Inhomogeneities in sequencing errors**

295 We further investigated the errors introduced during Illumina sequencing by characterizing the error
 296 profile of reads mapped to PhiX, a common spike-in used as sequencing control and for color balancing.
 297 For our analysis, we consider PhiX – a PCR-free, adapter-ligated sample derived from genomic DNA⁴⁰
 298 – essentially error-free and attribute all errors in its sequencing data to the sequencer. Using the eight
 299 PhiX datasets generated during sequencing on the Illumina iSeq 100 sequencer, we found substitutions
 300 are dominating, at $1.8 \pm 0.8 \cdot 10^{-3} \text{ nt}^{-1}$ on average, versus $< 0.1 \cdot 10^{-3} \text{ nt}^{-1}$ for both deletions and insertions.

301 This is in-line with other reports for other SBS-based sequencers^{21,22,41} and the analysis of non-
302 consensus errors between paired reads in our datasets (see Supplementary Figure 15). The
303 substitution rates in our experiments differed substantially between forward ($1.1 \pm 0.3 \cdot 10^{-3}$ nt⁻¹) and
304 reverse reads ($2.5 \pm 0.6 \cdot 10^{-3}$ nt⁻¹), and were strongly cycle-dependent (see Fig. 5a). They declined rapidly
305 towards a minimum around cycle 20, which coincides well with the calculations for phasing/pre-
306 phasing and colour-matrix corrections occurring at cycle 25.⁴² After cycle 25, the number of
307 substitutions consistently, but slowly increased each cycle (see Fig. 5a).

308 The substitutions introduced during sequencing showed a clear bias towards base transitions (e.g.
309 A↔G and C↔T) over transversions (all other combinations, see Fig. 5b), which differed slightly
310 between forward and reverse reads. Moreover, the increase in substitution rate after cycle 20 appears
311 to be primarily caused by A→T and T→G substitutions, while all other substitution patterns remain
312 nearly constant throughout the duration of the sequencing run (see Supplementary Figure 16). The
313 comparison to the base-calling method used in the iSeq's one-dye sequencing (see Fig. 5b, inset) shows
314 that base transitions correspond to false positive and false negative calls in the primary image,
315 accounting for 54% of all sequencing errors on average. A major exception is the A→T transition,
316 responsible for an additional 17±5% and 37±5% of substitutions in the forward and reverse reads
317 respectively, which corresponds to a false positive in the secondary image. Thus, unlike for sequencers
318 with other dye chemistries,²² substitution bias on the iSeq 100 appears to be related to its base-calling
319 matrix. Underlining this, substitutions involving miscalling intensities in both images ("cross-over" in
320 Fig. 5b) were rare and accounted for only 15% of substitution errors. Additionally, the analysis of non-
321 consensus errors between paired reads in our datasets (see Supplementary Figure 15) suggests that
322 polymerase errors during clonal amplification (i.e., the clustering step in SBS) also skew the
323 substitution bias.



324

325 **Fig. 5: Errors and biases from Illumina sequencing.** (a) Substitution rate during sequencing on the Illumina iSeq 100,
 326 estimated from the PhiX reads obtained during all sequencing experiments. Points show the individual substitution rate of
 327 the forward (dark blue) and reverse reads (light blue) at every position, with their respective moving median (10 base window,
 328 black lines). Only the positions until cycle 112 are shown, as low base diversity in the priming regions of the co-sequenced
 329 oligonucleotides drastically skews base calling accuracy. (b) Base bias of substitutions occurring during sequencing in the
 330 forward (dark blue) and reverse reads (light blue), shown as fractions of the total substitutions. The one-dye sequencing
 331 system used by the iSeq 100 sequencer (inset) uses the fluorescence intensity in two separate images for base calling.⁴²
 332 Depending on which fluorescence signal is miscalled, false positive (solid), false negative (dashed), or cross-over (dotted)
 333 errors occur and introduce a substitution into the sequencing data. Error bars show the standard deviation of the sample.

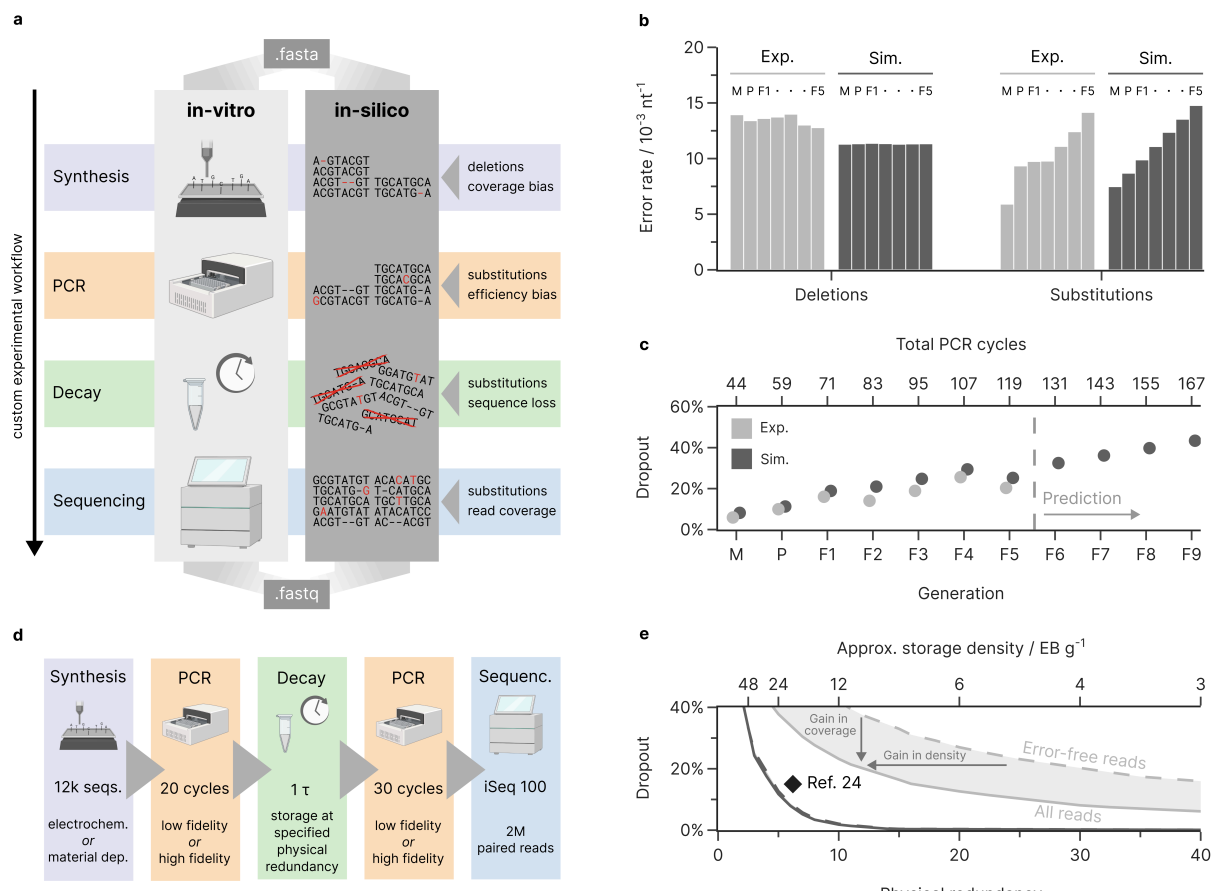
334 **A digital twin for DNA data storage**

335 Towards our goal of providing an accurate virtual representation of DNA data storage experiments, we
 336 implemented the error sources and biases characterized above into a digital twin of the DNA data
 337 storage process (see Fig. 6a). The digital twin's underlying model simulates all process steps (e.g.,
 338 synthesis, PCR) by stochastically introducing mutations into sequences at rates estimated from user-
 339 supplied experimental parameters. Specifically, we represent an oligonucleotide pool as a collection
 340 of sequences with associated abundances and use many oligonucleotides for each sequence to
 341 accurately represent the experimentally observed diversity of error patterns. Importantly, the biases
 342 introduced into the coverage distributions by synthesis, amplification, and dilution are also modelled

343 (e.g. by skewed initial distributions as in Fig. 2b, or non-homogeneous amplification as in Fig. 3d), so
344 that their negative effects on coverage homogeneity and sequence dropout are included. Additional
345 information and details on the implementation of each process step are given in the Methods and
346 Supplementary Note 2.

347 To assess our model's accuracy and versatility in predicting errors and biases from an experimental
348 workflow, we reproduced the experiments presented in this study (as internal validation) and
349 modelled the generational experiments by Koch et al.²⁵ (as external validation). These generational
350 experiments, starting from an electrochemically synthesized oligonucleotide pool, are ideal for model
351 validation: they consist of multiple dilutions and error-prone re-amplifications – exceeding 100 PCR
352 cycles in total – and include seven sequencing datasets for comparison. We observed good agreement
353 in the overall error rates and the coverage bias for both internal ($R^2_{\text{error}} = 0.98$, $R^2_{\text{bias}} = 0.74$, see
354 Supplementary Note 5) and external validation ($R^2_{\text{error}} = 0.87$, $R^2_{\text{bias}} = 0.64$, see Fig. 6b and
355 Supplementary Note 5). Notably, the experimental deletion rates in the generational experiments by
356 Koch et al.²⁵ exceeded the prediction of our model by about 20%, mostly due to differences in the
357 position-dependent deletion rates during synthesis (see Supplementary Figure 17). This difference is
358 likely caused by the implementation of process improvements by the synthesis provider sometime
359 between the study by Koch et al. and this work. This highlights the possible relevance of the digital
360 twin for the investigation of process deviations. Turning to coverage bias, we considered the rate of
361 sequence dropout – i.e., the ratio of original sequences which are no longer present in the sequencing
362 data – as our metric, due to its relevance for successful data recovery in a data storage context. We
363 found that our simulated sequencing data, downsampled to the original experiment's read counts,
364 accurately reproduced the sequence dropout observed over all seven generations (see Fig. 6c).
365 Importantly, had Koch et al.²⁵ been able to model their workflow, they would have been able to
366 increase storage capacity (by reducing redundancy) or lower costs (by synthesizing fewer sequences)
367 by more than threefold (the authors included redundancy for a sequence dropout of 80%, but a
368 maximum of 30% was required). Alternatively, using the model to forecast future generations of Koch's

369 experiment, at least four more generations would have been feasible at their redundancy level. This
 370 analysis highlights the value of the digital twin for the rational design of redundancy: it enables cost-
 371 saving optimizations and facilitates experimental planning.



372

373 **Fig. 6: Simulation of the DNA data storage channel.** (a) Overview of the developed model for the DNA data storage channel.

374 Experimental parameters for the synthesis, amplification, decay, and sequencing are used to replicate errors and biases in an

375 in-silico representation of an oligonucleotide pool. The order and parameters of all process steps can be customized to

376 describe user-defined workflows. (b+c) Verification of simulation results using the generational experiments reported by Koch

377 et al.²⁵ The mean error rates (b) and sequence loss (c) of the data storage workflow, as experimentally observed (light grey)

378 and as replicated in our model (dark grey), is shown for the master pool (denoted M), the parent (P), and all progeny

379 generations (F1 through F5). The model was also used to predict four further generations (F6 through F9). Datapoints are

380 slightly offset horizontally to prevent occlusion. Sequencing data from the model was downsampled to the read count in the

381 experimental sequencing data. (d+e) Simulation of the effects of physical coverage on sequences dropout in a best- and

382 worst-case scenario. By implementing a typical data storage workflow (d) using high- or low-fidelity process steps in our

383 model, the sequence dropout (e) as a function of physical redundancy is determined. The loss of sequences considering both

384 all sequencing reads (solid line) and only error-free reads (dashed line) is reported, with the shaded area in-between denoting

385 the improvement possible by error-correction coding. For comparison, the state-of-the-art storage density and redundancy
386 by Organick et al.²⁴ is shown (black diamond, 6.2x coverage at 15% data redundancy).

387 **Case study: optimal redundancy in extreme scenarios**

388 To highlight the value of modelling each process step for the design of redundancy in DNA data storage
389 systems, we implemented a prototypical storage workflow in our model as a case study. To investigate
390 optimal physical and logical redundancy, our prototypical workflow (see Fig. 6d) – involving post-
391 synthesis amplification, dilution to a specified physical coverage, storage for one half-live, re-
392 amplification, and sequencing – was further divided into two extreme cases. In our worst-case
393 scenario, an unconstrained, electrochemically synthesized oligonucleotide pool was used (see Fig. 2b)
394 together with a low-fidelity polymerase for PCR. Due to the highly skewed coverage and large error
395 rate, this scenario is representative of studies in which high redundancy is favoured and storage density
396 is not the main concern.^{9,25,43} In contrast, the best-case scenario utilized a narrowly distributed
397 oligonucleotide pool synthesized by a material deposition-based process, and further used a high-
398 fidelity polymerase for amplification. This is a low-error, low-bias scenario like those used in many
399 studies on ECC.^{8,12} As expected, our model predicted that the physical redundancy used during storage,
400 i.e., the effectively achieved storage density, strongly influences the sequence loss in both our
401 scenarios (see Fig. 6e). The less biased best-case scenario yielded near-complete recovery (98%) of
402 error-free sequences with only 10 copies per sequence during storage, corresponding to a storage
403 density close to the experimentally demonstrated state-of-the-art (6.2x coverage, 15%
404 redundancy).^{23,24} In contrast, the worst-case scenario lost 24% of all sequences at the same physical
405 redundancy, highlighting the importance of coverage homogeneity for high-density DNA data storage.

406 Logical redundancy implemented into an ECC provides two main benefits: first, it tolerates the loss of
407 a certain number of sequences (via); second, it enables the use and decoding of erroneous reads if no
408 error-free reads of a sequence are available (via within-sequence redundancy). The latter benefit
409 effectively yields either a gain in storage density or a gain in sequence coverage, as shown when
410 moving from the curve considering only error-free reads (naïve encoding, no within-sequence

411 redundancy) to all reads (ideal ECC, capable of decoding every erroneous read) in Fig. 6e. To take full
412 advantage of this gain in density or coverage, an ECC would have to be able to correct up to two
413 deletions and two substitutions per sequence in our low-fidelity scenario. However, our model shows
414 that even just the capability to correct up to two substitutions would approximately double the
415 number of eligible reads, as deletions are clustered in only 48% of reads (see Fig. 1d). In contrast, the
416 implementation of such within-sequence error correction would prove wasteful in our high-fidelity
417 scenario. There, considering only error-free reads does not significantly deteriorate sequence
418 coverage, as 81% of reads are error-free on average anyway. Consequently, a naïve encoding without
419 within-sequence redundancy will achieve a higher storage density in the best-case scenario than any
420 other ECC in the worst-case scenario, independently of the ECC's capabilities.

421 **Discussion**

422 The lack of comprehensive data on error rates, error homogeneity, and coverage biases throughout
423 the DNA data storage workflow has impeded the optimal design of ECCs and their parameters, as well
424 as hindered the comparison of ECC implementations. In this work, we have comprehensively
425 quantified errors and biases in DNA storage systems and developed a digital twin for modelling state-
426 of-the-art data storage workflows. Systematic sequencing of oligonucleotide pools during processing
427 showed that synthesis and standard PCR account for most deletions and substitutions, which
428 outnumber insertions by a factor of >10. Deletions were almost exclusively introduced by synthesis
429 and heterogeneously distributed in clusters. All other processing steps – amplification via PCR, aging,
430 and sequencing by SBS – added substitutions at varying rates, which were homogeneously distributed
431 but biased towards certain substitution patterns. Remarkably, the state-of-the-art data storage
432 workflow has become close to error-free (up to 87% of forward reads without error, 96% deletion-
433 free), as shown in our idealized high-fidelity storage scenario (see Fig. 6d). This implies some of the
434 ongoing optimization of ECCs towards increased error resilience to be better suited for applications in
435 which low-fidelity synthesis or sequencing processes require an ECC capable of utilizing highly
436 erroneous reads.^{43,44} In contrast, the commonly used workflow for high-density DNA data storage –
437 based on synthesis via material deposition and high-fidelity PCR – does not appear to benefit from
438 such ECC optimizations, as storage density is currently limited by coverage biases.

439 Synthesis and amplification also emerged as the major contributors to skewed coverage distributions
440 in our systematic analysis of coverage bias in synthetic oligonucleotide pools. While unoptimized
441 synthesis processes and the stochasticity of amplification are known to affect the coverage
442 distribution,²³ we identified both a striking difference in coverage uniformity between two different
443 synthesis processes and an apparent bias in the amplification efficiency during PCR. The consideration
444 of these coverage biases was shown to be crucial for understanding sequence dropout, a vital metric
445 for error-free readout due its severe effect compared to single mutations – necessitating redundant
446 sequences rather than just redundant symbols.

447 Our experimentally verified digital twin showcased the value of a customizable digital representation
448 of the DNA data storage process for experimental planning and the ECC design. The digital twin
449 facilitated the design of redundancy both in a literature scenario and a case study, which was shown
450 to translate into tangible cost savings. Furthermore, it highlighted that sequence dropout caused by
451 coverage bias, rather than erroneous sequences caused by mutations, is currently the limiting factor
452 in designing DNA data storage systems with increasingly higher storage densities. To this end, novel
453 approaches to remedy sequence dropout – such as ECCs capable of utilizing partial sequences⁴⁵ or
454 methods for enzymatic DNA repair³⁸ – will be invaluable to facilitate long-term storage at these high
455 storage densities.

456 Key limitations of our study include the consideration of only two commercial providers for synthesis
457 and only Illumina's SBS technology for sequencing. While these technologies are currently the most
458 relevant and widely-used,^{1,9} other emerging technologies – such as photoarray-based or enzymatic
459 synthesis, as well as nanopore sequencing – are expected to soon become relevant cost-effective
460 alternatives despite their lower fidelity.^{3,43,44} Furthermore, the broad scope of our analysis precluded
461 a detailed investigation into individual error sources, such as the effects of different polymerases or
462 correlations with sequence properties (e.g. GC content, homopolymers). Despite these limitations, we
463 hope both our error characterisation and our digital twin will help standardize the comparison and
464 accelerate the development of ECCs, as well as assist users in designing redundancy and experimental
465 workflows. For this, we provide a web platform to simulate both standardized and customized storage
466 scenarios at dt4dds.ethz.ch, as well as source code for fully custom workflows at github.com/fml-ethz/dt4dds. We also invite others to extend our model with more data, especially for the emerging,
468 low-fidelity technologies previously mentioned.

469 **Methods**

470 **Reagents**

471 Electrochemically synthesized oligonucleotide pools were ordered from CustomArray Inc. (Redmond,
472 WA, United States) and Genscript Biotech Corp. (Piscataway, NJ, United States) and used as delivered.
473 Material deposition-based oligonucleotide pools were synthesized by Twist Bioscience (San Francisco,
474 CA, United States) and resuspended to 10 ng μ L⁻¹ in ultrapure water. Primers were purchased from
475 Microsynth AG (Balgach, Switzerland). All pools and primers were further diluted as required with
476 ultrapure water. Additional details about the design of oligonucleotide pools and primers are given in
477 Supplementary Tables 1 and 2. KAPA SYBR FAST polymerase master mix was purchased from Sigma-
478 Aldrich (St. Louis, MI, United States).

479 **PCR and sequencing preparation**

480 Unless otherwise noted, 5 μ L of an oligonucleotide pool and 1 μ L each of the forward and reverse
481 primers (0F/0R, 10 μ M) were added to 10 μ L of 2x KAPA SYBR FAST master mix. Ultrapure water was
482 added up to a final volume of 20 μ L. Amplification by PCR used an initial denaturation at 95°C for 3
483 min, followed by cycles at 95°C for 15 s, 54°C for 30 s, and 72°C for 30 s. Cycling was stopped as soon
484 as the fluorescence intensity reached its plateau to prevent resource exhaustion, except for
485 quantitative PCR (calibration curves are given in Supplementary Figure 11). For sequencing
486 preparation, indexed Illumina adapters were added by PCR with overhang primers (2FUF/2RIF, 7-9
487 cycles, see Supplementary Table 2). The PCR product from each well was then run on an agarose gel
488 (E-Gel EX Agarose Gels 2%, Invitrogen) with a 50 bp ladder (Invitrogen), and the appropriate band was
489 purified (ZymoClean Gel DNA Recovery Kit, ZymoResearch) before quantification by fluorescence
490 (Qubit dsDNA HS Kit, Invitrogen).⁹

491 **Sequencing**

492 For each sequencing run, 5-6 samples were individually diluted to 1 nM and pooled. The pooled sample
493 was further diluted to 50 pM. Then, 2% PhiX (PhiX Control v3, Illumina) was spiked into the sample and
494 20 μ L were added to an Illumina iSeq 100 i1 Reagent v2 cartridge. 150 nt paired-end sequencing with

495 the Illumina iSeq 100 sequencer yielded between 4-5 million reads, leading to an average sequencing
496 coverage of 90 paired reads per sequence.

497 **Protocol for amplification experiments**

498 For the amplification experiments, oligonucleotide pools were sequentially amplified and diluted
499 multiple times under the same conditions to yield samples at six different PCR cycle counts. For this,
500 the pools synthesized by material deposition (500x dilution) were amplified in two wells each, one well
501 containing standard primers (0F/0R) and one containing the indexed overhang primers with
502 sequencing adapters (2FUF/2RIF). After 15 cycles, the PCR product with sequencing adapters was
503 stored at -20°C. 1 μ L of the PCR product with the standard primers was diluted by 3800x, and 5 μ L were
504 used for the next round of amplification (for a total dilution of 15200x, equivalent to 1.9^{15} , the expected
505 amplification factor after 15 PCR cycles with 90% efficiency). If the fluorescence observed in the last
506 cycle of an amplification round was approaching the plateau value, the dilution for the next round was
507 increased two-fold, i.e., to 7600x. This sequential procedure was performed for a total of six rounds,
508 yielding samples with 15 to 90 PCR cycles. The PCR products with sequencing adapters were then
509 prepared for sequencing (see above) without the additional indexing step. The workflow is shown in
510 Supplementary Figures 18 and 19.

511 The procedure and results for the amplification experiments of the electrochemically synthesized
512 pools (not shown in Fig. 3) are given in Supplementary Note 4. The workflow is illustrated in
513 Supplementary Figures 20 and 21.

514 **Protocol for storage experiments**

515 Both the electrochemically synthesized pools (50x dilution) and the pools synthesized by material
516 deposition (1000x dilution) were first amplified for 20-21 cycles, using 96 wells each and 1 μ L sample
517 per well. Then, all wells from each pool were pooled and purified (DNA Clean & Concentrator-5,
518 ZymoResearch) to yield stock solutions with 30-50 ng μ L⁻¹ dsDNA in ultrapure water. Of these, 30 ng
519 each were added to microcentrifuge tubes and dried in vacuo for 30 min at 45°C. After drying, one set
520 of tubes was immediately stored at -20°C to represent the unaged reference sample. For accelerated

521 aging, all other samples were stored in a desiccator over saturated sodium bromide in water (>99%,
522 Roth AG) at 70°C and 50% relative humidity.⁷ Samples were moved to -20°C storage after around two,
523 four and seven days, with each time point at least in triplicate. All samples were resuspended in 200
524 µL ultrapure water and quantified by qPCR to yield a decay curve, as described below. Calibration
525 curves for this qPCR analysis were previously established by serial dilution of the stock solutions and
526 are shown in Supplementary Figure 11 with their parameters given in Supplementary Table 3. For the
527 decay curve, the concentration of all samples was normalized to the mean concentration of the unaged
528 reference sample, and then fitted to a first-order decay model according to:

529

$$\frac{c(t)}{c(0)} = e^{-kt}, \text{ where } k = \frac{\ln 2}{\tau}.$$

530 The decay curves and their parameters are given in Supplementary Figure 11 and Supplementary Table
531 4, respectively.

532 For sequencing, all samples were diluted to the concentration of the sample at seven days to
533 circumvent any dilution effects, amplified for 16-18 cycles, and then underwent the standard
534 sequencing preparation (see above). The workflow is shown in Supplementary Figures 23-26. To
535 normalize the extent of decay across the four oligonucleotide pools for the estimation of error rates
536 during aging, the number of half-lives, determined as the storage duration relative to the half-live, was
537 used. The conversion for all timepoints is given in Supplementary Table **Error! Reference source not**
538 **found.**⁵.

539 **Read mapping and error analysis**

540 To estimate error rates from sequencing reads, up to 1 million paired-end sequencing reads were first
541 mapped to their respective reference sequence using a custom Python script, and then filtered to
542 exclude reads with less than 85% similarity to their reference. This filtering threshold was chosen based
543 on similarity comparisons between experimental and random datasets (see Supplementary Figure 1).
544 From the resulting mappings, error rates as a function of position, involved bases, read direction, and
545 error length were derived and used for further data analysis. Coverage distributions were derived from

546 the alignment counts given by sequence alignment with BBMap⁴⁶ after adapter trimming and
547 normalization to the mean oligonucleotide coverage. Lognormal distributions were fitted to the
548 normalized coverage distributions to help with visualization, and the corresponding standard deviation
549 of the lognormal distribution is shown to quantify the coverage bias. Full details are given in
550 Supplementary Note 2 and the complete source code is publicly available in the GitHub repository (see
551 Code Availability statement).

552 **ANOVA and error independence**

553 Three-way ANOVA ($n = 80$) with the factors synthesis provider, number of PCR cycles, and days of
554 storage was performed using type II sum of squares, heteroskedasticity-consistent standard errors
555 (HC3) and without interactions. The analysis was performed for each error type independently and
556 according to the following linear model:

557
$$\text{Error rate} \sim C(\text{synthesis}) + \#\text{PCR cycles} + \#\text{Days of storage}$$

558 For the analysis of error independence, theoretical probability mass functions under the assumption
559 of error independence were independently calculated for each pool and experiment. For the
560 probability mass function of consecutive errors, a geometric distribution parameterized by the mean
561 error rate was used, i.e. $n \sim \text{Geom}(1 - \text{mean error rate})$. For the probability mass function of errors
562 per read, a binomial distribution parameterized by the length of the sequence and the mean error rate
563 was used, i.e. $n \sim \text{Binom}(\text{length}, \text{mean error rate})$.

564 **Modelling of the DNA data storage process**

565 The model used for the simulation of the DNA data storage process, implemented in Python, consists
566 of a hash map representing a pool of oligonucleotides, error generators introducing mutations at
567 specified rates and with certain biases, and classes encapsulating the error generators into the
568 individual process steps (i.e. synthesis, PCR, storage, and sequencing). Starting from a set of reference
569 sequences and an experimental workflow provided by the user, the model simulates errors and biases
570 and ultimately yields artificial sequencing data in the FASTQ format for further use. The individual error
571 sources and coverage biases of each process step are reproduced based on user-defined experimental

572 parameters (e.g. synthesis provider, choice of polymerase, storage duration) and the error rates and
573 biases quantified in this study. Coverage bias is implemented both during synthesis – via skewed initial
574 count distributions as in Fig. 2d – and during amplification, using normally-distributed relative
575 amplification efficiencies as in Fig. 3d. Additionally, amplification is implemented as a branching
576 binomial process, based on oligonucleotide count and the sequence’s amplification efficiency, to
577 account for the stochastic effects observed at low coverage.^{23,29} Dilution, sequencing, and decay are
578 modelled as random sampling, in-line with the findings in Fig. 4 and the literature.^{6,23} Full details are
579 given in Supplementary Note 2 and the complete source code is publicly available in the GitHub
580 repository (see Code Availability statement).

581 **Internal and external validation**

582 For the internal validation, all experimental conditions from this study were recreated with our tool
583 and the simulated sequencing data underwent identical post-processing and error analysis. Only the
584 position-, length-, and base-dependent error rates, process-specific error patterns, and coverage
585 biases characterized in this study were utilized. Due to small differences in the positional deletion rates
586 between the two electrochemically synthesized pools, pool-specific deletion rates were used (see
587 Supplementary Note 3) rather than the overall deletion rate presented in Fig. 2a.

588 For the external validation, the workflow for the generational experiments by Koch et al.²⁵ was
589 reproduced with our tool to the extent possible given the information provided in their study.
590 Electrochemical synthesis was assumed with positional error rates as in Fig. 2a, and a coverage bias of
591 $\sigma = 0.94$ (mean of GC-constrained and unconstrained pools, see Fig. 2b) due to their use of a partially
592 GC-constraining ECC. Amplification by PCR assumed a Taq-based polymerase with an amplification bias
593 as estimated for the Koch et al. experiments in Fig. 3d (i.e., $\sigma = 0.012$). Missing information about
594 dilutions were estimated from other protocols⁹ and the number of PCR cycles used. For the analysis in
595 Fig. 6c, only error-free reads were used – as in the original study – and the simulated sequencing data
596 was downsampled to the same read count as the experimental data to ensure comparability. For the
597 generations F6-F9, the average read count of generations M-F5 was assumed.

598 More details on the parameters and results for both internal and external validation are presented in
599 Supplementary Note 5. The scripts for both internal and external validation are also provided with the
600 code in the repository for reproducibility.

601 **Case study on storage density**

602 The best- and worst-case scenarios implemented in our tool were both based on the error
603 characterization in this study and common experimental workflows for high-density DNA data
604 storage.^{8,10,13,24} The scenarios followed an identical workflow (see Fig. 6d and below) consisting of
605 synthesis, amplification, storage, re-amplification, and sequencing. Specifically, 12000 sequences were
606 synthesized at a mean coverage of 200, underwent 20 PCR cycles with an amplification bias of $\sigma =$
607 0.0051 (see Fig. 3c), were stored for one half-life at mean coverages ranging from 0.5-50
608 oligonucleotides per sequence, amplified for another 30 cycles, and finally sequenced with the iSeq
609 100. In the best-case scenario, the coverage bias and error rate of the material deposition-based
610 synthesis (see Fig. 2), and the polymerase fidelity of Q5 High-Fidelity DNA Polymerase (i.e., 280)²⁰ were
611 used. In the worst-case scenario, the coverage bias and error rate of electrochemical synthesis, and
612 the fidelity of a Taq-based polymerase (i.e., 1) were used instead. For the analysis in Fig. 6e, either all
613 or only error-free reads (see Supplementary Note 1) were used to determine the sequence dropout in
614 both cases, equivalent to an ideal ECC, and a naïve ECC, respectively. The script for this case study is
615 provided with the code in the repository for full documentation of the parameters.

616

617 **References**

- 618 1. Ceze, L., Nivala, J. & Strauss, K. Molecular digital data storage using DNA. *Nat. Rev. Genet.* **2019**
619 **208** **20**, 456–466 (2019).
- 620 2. Church, G. M., Gao, Y. & Kosuri, S. Next-generation digital information storage in DNA. *Science*
621 **337**, 1628 (2012).
- 622 3. Dorigchi, A. *et al.* Emerging Approaches to DNA Data Storage: Challenges and Prospects. *ACS*
623 *Nano* (2022) doi:10.1021/acsnano.2c06748.
- 624 4. Reinsel, D., Gantz, J. & Rydning, J. *The Digitization of the World: From Edge to Core.*
625 (International Data Corporation #US44413318, 2018).
- 626 5. DNA Data Storage Alliance. *Preserving our digital legacy: An introduction to DNA data storage.*
627 (2021).
- 628 6. Heckel, R., Mikutis, G. & Grass, R. N. A Characterization of the DNA Data Storage Channel. *Sci.*
629 *Rep.* **2019** **91** **9**, 1–12 (2019).
- 630 7. Antkowiak, P. L. *et al.* Integrating DNA Encapsulates and Digital Microfluidics for Automated Data
631 Storage in DNA. *Small* **2107381** (2022) doi:10.1002/SMIL.202107381.
- 632 8. Erlich, Y. & Zielinski, D. DNA Fountain enables a robust and efficient storage architecture. *Science*
633 **355**, 950–954 (2017).
- 634 9. Meiser, L. C. *et al.* Reading and writing digital data in DNA. *Nat. Protoc.* **2019** **151** **15**, 86–101
635 (2019).
- 636 10. Grass, R. N., Heckel, R., Puddu, M., Paunescu, D. & Stark, W. J. Robust Chemical Preservation of
637 Digital Information on DNA in Silica with Error-Correcting Codes. *Angew. Chem. Int. Ed.* **54**, 2552–
638 2555 (2015).
- 639 11. Schwarz, P. M. & Freisleben, B. NOREC4DNA: using near-optimal rateless erasure codes for DNA
640 storage. *BMC Bioinforma.* **2021** **221** **22**, 1–28 (2021).
- 641 12. Ping, Z. *et al.* Towards practical and robust DNA-based data archiving using the yin–yang codec
642 system. *Nat. Comput. Sci.* **2022** **24** **2**, 234–242 (2022).

643 13. Welzel, M. *et al.* DNA-Aeon provides flexible arithmetic coding for constraint adherence and
644 error correction in DNA storage. *Nat. Commun.* **14**, 628 (2023).

645 14. Chaykin, G., Furman, N., Sabary, O., Ben-Shabat, D. & Yaakobi, E. DNA-Storalator: End-to-End
646 DNA Storage Simulator, in *13th Annual Non-Volatile Memories Workshop* (2022).

647 15. Yuan, L., Xie, Z., Wang, Y. & Wang, X. DeSP: a systematic DNA storage error simulation pipeline.
648 *BMC Bioinforma.* 2022 **231** **23**, 1–14 (2022).

649 16. Schwarz, M. *et al.* MESA: automated assessment of synthetic DNA fragments and simulation of
650 DNA synthesis, storage, sequencing and PCR errors. *Bioinformatics* **36**, 3322–3326 (2020).

651 17. Filges, S., Mouhanna, P. & Ståhlberg, A. Digital Quantification of Chemical Oligonucleotide
652 Synthesis Errors. *Clin. Chem.* **67**, 1384–1394 (2021).

653 18. Kosuri, S. & Church, G. M. Large-scale de novo DNA synthesis: technologies and applications.
654 *Nat. Methods* **11**, 499–507 (2014).

655 19. Shagin, D. A. *et al.* A high-throughput assay for quantitative measurement of PCR errors. *Sci. Rep.*
656 2017 **71** **7**, 1–11 (2017).

657 20. Potapov, V. & Ong, J. L. Examining Sources of Error in PCR by Single-Molecule Sequencing. *PLOS*
658 *ONE* **12**, e0169774 (2017).

659 21. Schirmer, M., D'Amore, R., Ijaz, U. Z., Hall, N. & Quince, C. Illumina error profiles: resolving fine-
660 scale variation in metagenomic sequencing data. *BMC Bioinformatics* **17**, 125 (2016).

661 22. Stoler, N. & Nekrutenko, A. Sequencing error profiles of Illumina sequencing instruments. *NAR*
662 *Genomics Bioinforma.* **3**, (2021).

663 23. Chen, Y.-J. *et al.* Quantifying molecular bias in DNA data storage. *Nat. Commun.* 2020 **111** **11**, 1–9
664 (2020).

665 24. Organick, L. *et al.* Random access in large-scale DNA data storage. *Nat. Biotechnol.* 2018 **363** **36**,
666 242–248 (2018).

667 25. Koch, J. *et al.* A DNA-of-things storage architecture to create materials with embedded memory.
668 *Nat. Biotechnol.* 2019 **381** **38**, 39–43 (2019).

669 26. Xu, C. *et al.* Electrochemical DNA synthesis and sequencing on a single electrode with scalability
670 for integrated data storage. *Sci. Adv.* **7**, eabk0100 (2021).

671 27. Nguyen, B. H. *et al.* Scaling DNA data storage with nanoscale electrode wells. *Sci. Adv.* **7**, 6714
672 (2021).

673 28. McInerney, P., Adams, P. & Hadi, M. Z. Error Rate Comparison during Polymerase Chain Reaction
674 by DNA Polymerase. *Mol. Biol. Int.* **2014**, e287430 (2014).

675 29. Best, K., Oakes, T., Heather, J. M., Shawe-Taylor, J. & Chain, B. Computational analysis of
676 stochastic heterogeneity in PCR amplification efficiency revealed by single molecule barcoding.
677 *Sci. Rep.* **2015** *51* 5, 1–13 (2015).

678 30. Gao, Y., Chen, X., Qiao, H., Ke, Y. & Qi, H. Low-Bias Manipulation of DNA Oligo Pool for Robust
679 Data Storage. *ACS Synth. Biol.* **9**, 3344–3352 (2020).

680 31. Kebschull, J. M. & Zador, A. M. Sources of PCR-induced distortions in high-throughput
681 sequencing data sets. *Nucleic Acids Res.* **43**, e143 (2015).

682 32. Aird, D. *et al.* Analyzing and minimizing PCR amplification bias in Illumina sequencing libraries.
683 *Genome Biol.* **12**, 1–14 (2011).

684 33. Mallona, I., Weiss, J. & Marcos, E. C. PcrEfficiency: A Web tool for PCR amplification efficiency
685 prediction. *BMC Bioinforma.* **12**, 1–7 (2011).

686 34. Pan, W. *et al.* DNA polymerase preference determines PCR priming efficiency. *BMC Biotechnol.*
687 **14**, 1–17 (2014).

688 35. Dabney, J. & Meyer, M. Length and GC-biases during sequencing library amplification: A
689 comparison of various polymerase-buffer systems with ancient and modern DNA sequencing
690 libraries. *BioTechniques* **52**, (2012).

691 36. Greagg, M. A. *et al.* A read-ahead function in archaeal DNA polymerases detects promutagenic
692 template-strand uracil. *Proc. Natl. Acad. Sci.* **96**, 9045–9050 (1999).

693 37. Lett, B. *et al.* Oligo replication advantage driven by GC content and Gibbs free energy.
694 *Biotechnol. Lett.* **2022** 1–11 (2022) doi:10.1007/S10529-022-03295-2.

695 38. Meiser, L. C. *et al.* Information decay and enzymatic information recovery for DNA data storage.

696 *Commun. Biol.* **5**, 1–9 (2022).

697 39. Mikutis, G., Schmid, L., Stark, W. J. & Grass, R. N. Length-dependent DNA degradation kinetic

698 model: Decay compensation in DNA tracer concentration measurements. *AIChE J.* **65**, 40–48

699 (2019).

700 40. What is the PhiX Control v3 Library and what is its function in Illumina Next Generation

701 Sequencing. [https://knowledge.illumina.com/library-preparation/general/library-preparation-](https://knowledge.illumina.com/library-preparation/general/library-preparation-general-reference_material-list/000001545)

702 [general-reference_material-list/000001545](https://knowledge.illumina.com/library-preparation/general/library-preparation-general-reference_material-list/000001545) (accessed 28.06.2023).

703 41. Ross, M. G. *et al.* Characterizing and measuring bias in sequence data. *Genome Biol.* **14**, 1–20

704 (2013).

705 42. Illumina Inc. *iSeq 100 Sequencing System*. (Document #200015511 v00, 2022).

706 43. Antkowiak, P. L. *et al.* Low cost DNA data storage using photolithographic synthesis and

707 advanced information reconstruction and error correction. *Nat. Commun.* **2020** **11** **11**, 1–10

708 (2020).

709 44. Lopez, R. *et al.* DNA assembly for nanopore data storage readout. *Nat. Commun.* **2019** **10** **10**, 1–

710 9 (2019).

711 45. Bar-Lev, D., Marcovich, S., Yaakobi, E. & Yehezkeally, Y. Adversarial Torn-paper Codes. in **2022**

712 *IEEE International Symposium on Information Theory (ISIT)* 2934–2939 (2022).

713 doi:10.1109/ISIT50566.2022.9834766.

714 46. Bushnell, B. BBMap: A Fast, Accurate, Splice-Aware Aligner. *SourceForge*

715 <https://sourceforge.net/projects/bbmap/> (2022).

716

717

718 **Acknowledgments**

719 This project was financed by the European Union's Horizon 2020 Program, FET-Open: DNA-
720 FAIRYLIGHTS, Grant Agreement No. 964995. We thank Dr. Max Horn and Dr. Philipp Antkowiak for the
721 fruitful discussions which motivated this study, as well their input on method development. Data
722 analysis and simulations were performed on the Euler cluster operated by the High-Performance
723 Computing group at ETH Zürich. Figures were partially created with BioRender.com.

724 **Author contributions**

725 R.N.G. and R.H. initiated and supervised the project with input from W.J.S. A.L.G. performed the
726 experiments, developed the code, performed data analysis, prepared illustrations, and wrote the
727 manuscript with input and approval from all authors.

728 **Competing interests**

729 The authors declare no competing financial interest.

730 **Data availability**

731 Both the experimental and simulated sequencing data underlying the findings of this study are
732 openly available at doi.org/10.6084/m9.figshare.c.6717855. Sequencing data from the studies by
733 Koch et. al., Erlich et. al., and Organick et. al. are available from references 8, 23, and 25.

734 **Code availability**

735 The code for error analysis and simulation of the DNA data storage process is deposited in the public
736 GitHub repository at github.com/fml-ethz/dt4dds. The code for data analysis, in the form of Jupyter
737 Notebooks and data files, is deposited in the public GitHub repository at github.com/fml-ethz/dt4dds_notebooks.

739 **Additional Information**

740 Supplementary Information is available for this paper.

741 Correspondence and requests should be addressed to Robert N. Grass.